RSC Advances

RSC Advances

www.rsc.org/advances

ROYAL SOCIETY OF CHEMISTRY

www.rsc.org/advances

RSC Advances

RSC Advances

ARTICLE

Nitrogen-enriched activated carbons from waste particleboard used as electrode materials for supercapacitors: Effects of activating agent on surface characteristics

T. X. Shang,[a] J. Zhang,[a] F. L. Fan[a] and X. J. Jin[a, *]

Abstract: Nitrogen-enriched activated carbon was prepared from waste particleboard by a chemical activation method, where partially carbonized waste particleboard was treated with KOH in different ratio. The porosity and nitrogen content of the nitrogen-enriched activated carbons depend strongly on the weight ratio of KOH/carbonization. As the weight ratio of KOH/carbonization increases from 2 to 5, the specific surface area increases from 1498 to 1826 m^2 g^{-1}, while the nitrogen content decreases from 2.86 to 1.32 *wt*.%.. These nitrogen-enriched activated carbons are tested as electrode material in two-electrode symmetric supercapacitor system in 7 M KOH electrolyte and found to exhibit high specific capacitance with excellent retention of it at high current density and for long term operation. In particular, the nitrogen-enriched activated carbon prepared with a moderate KOH/carbonization weight ratio of 3, which possesses a balanced specific surface area (1758 m^2 g^{-1}) and nitrogen content (2.38 *wt*.%) exhibits the largest specific capacitance of 263 F g^{-1} at 0.05 A g^{-1}, attributed to the co-contribution of double-layer capacitance and pseudo-capacitance. Moreover, it shows excellent rate capability (228 F g^{-1} at 10 A g^{-1}) and good cycling stability (over 95% capacitance retention over 3000 cycles), making it a promising electrode material for supercapacitors.

Introduction

Supercapacitors, which are also known as ultracapacitors or electrochemical capacitors, are the energy storage devices that possess high power density (10 kW kg^{-1}), which can be fully charged or discharged in seconds.[1] In terms of their performance, they can strategically fill in the gap between conventional capacitors and batteries to give better energy and power performance. The potential applications of supercapacitors vary from household electronic products to emergency doors in Airbus A380 planes[2, 3] owing to their excellent energy and power performance. Based on the charge-storage mechanism, supercapacitors can be divided into two categories: Pseudo-capacitors and Electrical double-layer capacitors (EDLCs).[4-10] Pseudo-capacitors, in which metal oxides and conducting polymers are used as the main types of electrode materials,[6, 11-13] store electrical energy faradaically through electrosorption, reduction-osidation reactions, and intercalation processes.[5] Another class of supercapacitors, EDLCs, which usually employ porous carbons as the electrode materials, store energy by exploiting the charge separation at electrode/electrolyte interfaces.[5] Today, commercial supercapacitors are dominated by EDLCs with activated carbon (AC) as the electrode material due to the high microporosity and low cost.[14, 15] However, the specific capacitance is relatively low and an evident decrease in capacitance is observed at high current density, resulting in low energy density, which limits their further application.[16]

Of particular note, chemical attributes still play a significant role in determining the capacitive performance of the AC-based electrodes, besides specific surface area, pore geometry and electrical conductivity.[17-20] As a result, an emerging alternative is to further modify AC materials with O-,[17, 21-22] N-[23-30] or P-containing functional groups,[19] which can considerably enhance the total specific capacitance through the additional pseudo-capacitance effects, as well as improving the wettablility of the AC-based electrode with the electrolyte meanwhile.[17-20] What's more, the N doping was also found to enhance the electronic conductivity of the AC material itself,[17-19, 23-31] favoring for the enhanced power property. K. Jurewicz et al.[32] investigated the capacitive performance of activated carbons (ACs) with different contents of nitrogen coming from urea, obtained from brown coal as a precursor and showed the nitrogen-enriched carbon can be successfully used as electrode materials in acidic and alkaline capacitors. M. Zhou et al.[6] prepared the nitrogen-doped porous carbon that possess a balanced specific surface area and nitrogen content and investigated that the large specific capacitance of the nitrogen-doped porous carbon is attributed to the co-contribution of double-layer capacitance and pseudo-

[a.] MOE Key Laboratory of Wooden Material Science and Application, Beijing Key Laboratory of Lignocellulosic Chemistry, MOE Engineering Research Center of Forestry Biomass Materials and Bioenergy, Beijing Forestry University, 35 Qinghua East Road, Haidian, 100083, Beijing, China.
* Corresponding author. Tel.: +8613718160441, Fax: None. E-mail address:jxj0322@163.com

capacitance. In order to design and fabricate the compact and portable energy storage devices, it is urgently required to synthesize AC-based electrode materials with high specific capacitance and good capacitance retention. Herein, we researched the capacitive performance of nitrogen-enriched ACs obtained from waste particleboards, which are bonded with formaldehyde-based adhesives, especially urea-formaldehyde (UF) adhesive.

Particleboard wastes are low-cost materials which have already been tested as attractive precursors for producing ACs from a two steps thermos-chemical process.[33] Furthermore, China is a big country in composite panel production and consumption, and there is a great quantity of composite panels (include particleboards) produced every year as the development of the economy. In addition, with the development of real estate, the demand of high-quality particleboard in wooden furniture industry is increasing. Therefore, the production of particleboard is constantly increasing. According to the reports, the production of particleboard was 18.8495 million cubic meters in China in 2013, and that showed an increase of 49.1 percent over the 12.642 million cubic meters in 2010.[34] However, the large numbers of particleboards were discarded. Currently, the common method to eliminate waste particleboards include: recycling,[35] open burning, land filling, and pyrolysis.[36] Nakai[37] reported that the low-temperature pyrolysis products of disused composite panels have higher application value than the pyrolysis products of ordinary wood materials. During the pyrolysis process, the inversion and fixing of nitrogen element coming from adhesives could endow the products with new properties.

In this paper, we utilized waste particleboards as the precursor to prepared nitrogen-enriched ACs. The effects of the KOH/carbonization weight ratio on the textural properties and capacitive performance of the ACs have been analyzed in detail. Additionally, the influence of nitrogen content and types of nitrogen functional groups on capacitive performance of nitrogen-enriched ACs has been investigated.

Experimental

The waste particleboards was kindly provided by Beijing Jiahekailai Furniture and Design Company, which was obtained in the furniture manufacturing process containing 10 % urea-formaldehyde resin adhesive of the mass. Other chemicals were analytical grades and were purchased from Beijing Lanyi Chemical reagent.

Preparation of nitrogen-enriched AC materials

The nitrogen-enriched ACs were simply prepared by waste particleboards in a furnace with the heating rate of 10 ℃ · min^{-1} up to a final temperature of 500 ℃ under N_2 protection for 60 min. Then the obtained carbides were grinded by a high-speed disintegrator and sifted out the particle diameter in

range of 40-60 grit numbers by standard sieve to get suitable samples for activation and designated as C500. Subsequently, in the impregnation-activation process, dried carbide scrap samples were mixed with 50% KOH solution with different mass ratio of 2, 3, 4, and 5 based on KOH, stirred and then settled in room for 16 h. The mixtures dried in an electric stove were to preserve activation temperature at 800 ℃ for 1 h in a tube furnace under N_2 protection. After cooling, the obtained ACs were boiled first with distilled water, then with 1 M HCl solution until the pH of solution reach to about 6-7, and dried at 105 ℃ in an oven for 8 h. The ACs finally obtained were designated as AC-x, where x represents the mass ratio of KOH and carbide, namely, AC-2, AC-3, AC-4, and AC-5.

Characterization of samples nitrogen-enriched ACs

The morphology of the samples was examined by using a field emission scanning electron microscopy (FE-SEM, SU8010, Hitachi). The specific surface area and pore size distribution of the activated carbons were determined using nitrogen adsorption-desorption isotherms at -196 ℃ (ASAP 2010, Micromeritics). The specific surface area (S_{BET}) was calculated by the conventional BET (Brunauer-Emmett-Teller) method. The pore size distribution was calculated by density functional theory (DFT) using a carbon slit pore equilibrium model. In addition, elemental analysis was conducted on a Vario EL III (Elementar Analysensysteme GmbH, Germany) to determine the total carbon and nitrogen content of the samples. The surface elemental composition was determined by X-ray photoelectron spectroscopy (XPS) technique using Axis Ultra high-performance imaging (Kratos Analytical Ltd. UK).

Fabrication of the supercapacitors

At first, the electrode was prepared by mixing nitrogen-enriched AC materials (87 *wt*.%), acetylene black (10 *wt*.%), and polytetrafluoro-ethylene (PTFE, 3 *wt*.%, as binder), using alcohol as solvent. Then, the as-prepared slurry was pressed onto a nickel foam current collector (1 cm × 1 cm) at 20 MPa and dried in a vacuum oven at 102 ℃. A symmetric supercapacitor was assembled by two electrodes separated by a porous membrane.

Electrochemical measurements

Galvanostatic charge-discharge, cyclic voltammetry (CV), electrochemical impedance spectroscopy (EIS), and cycle test were used to evaluate the electrochemical properties of nitrogen-enriched ACs with aqueous KOH solution (7 M) as the electrolyte. BT2000 battery testing system (Arbin Instruments, USA) and 1260 electrochemical workstation (Solartron Metrology, UK) was used to perform all the electrochemical measurements.

Results and discussion

Morphology and structure characterization

FE-SEM morphologies of C500, AC-2, AC-3, AC-4, and AC-5 are shown in Fig. 1, where highly irregular and rough surface stature originated from highly porous morphology can be observed for all the samples. But, on careful observation, we can see that the surface in AC samples are rougher with the addition of KOH usage. The C500 show thick mass shape and a smoothest surface with no porous. And the AC-5 possesses larger pores and flimsier carbon framework than AC-2, AC-3, and AC-4, illustrating it has been burned off as the excessive activation. Consequently, it is necessary to investigate the moderate KOH usage to obtain the ACs with highly developed pore structure. Fig. 2 shows the Raman spectra of all the AC samples. The peaks at 1350 and 1596 cm^{-1} are represented as the D-band and the G-band, respectively, which are characteristic Raman peaks for carbon materials[38, 39]. The ratio of the relative intensity of the D-band and G-band (I_D/I_G) is proportional to the number of defect sites in carbon[40]. The higher the ratio, the lower the degree of graphitization. For these AC samples, the I_D/I_G value of AC-3 (0.92) is the lowest, indicating that the degree of graphitization of AC-3 is the highest. Also the I_D/I_G values of other AC samples are 1.02, 0.95 and 1.00 for AC-2, AC-4, AC-5, respectively. The decrease of the degree of graphitization will lead the conductivity of the ACs to decrease. So finely tailoring the degree of graphitization and the porous microstructure of the ACs by controlling the KOH usage is crucial during KOH activation.
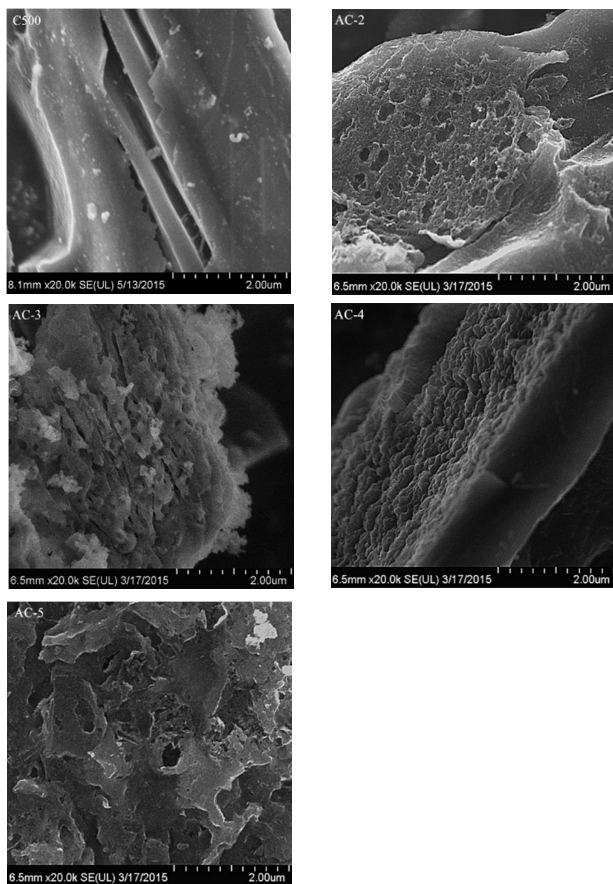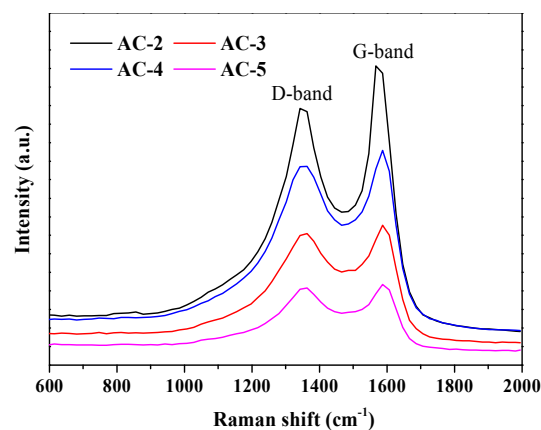
Fig. 2 Raman spectra of all AC samples.

It is known that KOH activation will introduce micro/meso-porous structures into the resulting carbon whose surface area and porosity can be tuned by the KOH usage. The textural properties of C500 and the different AC samples with different KOH usage (KOH/carbon of 2, 3, 4, and 5) were analyzed by means of N_2 adsorption at -196 ℃. The N_2 adsorption and desorption isotherms (Fig. 3(a)) show that both samples exhibit a characteristic type-I isotherm with slight hysteresis loop, indicating the presence of a large number of micropores and a certain amount of mesopores in all AC samples. Sharp increase in volume at low relative pressure also shows the microporosity. As Fig. 3(a) shows that activating obviously improved the porosity of C500. Besides, the desorption isotherms show the presence of hysteresis loops at relative pressures in excess of 0.4, which are characteristic of a Type-IV isotherm, which additionally substantiates the mesoporous nature of the samples. The pore size distribution calculated by the density functional theory (DFT), assuming a strong peak at about 0.85 nm and a weaker peak at about 1.2 nm for micropores and a wide cylindrical pore geometry for the mesopores, reveals the existence of well-defined micro- and meso-pores with sizes of less than 4 nm (Fig. 3(b)). However, the C500 nearly has no pores. At the same time, the isotherm for AC-4 of a maximum amount of N_2 adsorbed compared with AC-2, AC-3, and AC-5, this can be caused by two factors: the first is the collapse of adjacent micropores, thus leading to the formation of more mesopores under severe activation conditions for AC-5;[41, 42] the other is due to more heteroatom functional groups entrapped in the micropores, and thus, increasing the surface energy for AC-2 and AC-3.[43] AC-4 possessed the largest specific surface area (1826 $m^2\ g^{-1}$), whilst the specific surface areas of AC-2, AC-3, and AC-5 were 1498, 1758, and 1672 $m^2\ g^{-1}$, respectively. The pore volumes were 0.914, 1.169, 1.242, and 0.962 $cm^3\ g^{-1}$ for AC-2, AC-3, AC-4, and AC-5, respectively (Table 1). These results confirmed that the KOH/carbonization weight ratio was an important parameter for controlling the development of porosity in chemical activation.

Overnight stirring of char with KOH leads to a homogeneous mixture of them, and at high temperature KOH oxidatively reacts with char carbon to form H_2, CO_2 and CO gas and thus

Fig. 1. FE-SEM images of all AC samples.

COMMUNICATION

create the pores.[44] And it has been generally suggested that the activation reaction between KOH and carbon proceeds according to the eqn (1), followed by the decomposition of K_2CO_3 (eqn (2)) and/or the simultaneous reaction of $K/K_2CO_3/CO_2$ with carbon (eqn (3), (4), (5)). Overall, as the KOH usage increases, the gaseous product (H_2, CO_2, CO) increases, while the effect of pore-expanding is improved. As a result, the micropore volume (in Table 2) show an increase first and then a decrease with the increase of the KOH usage.

$$6KOH+2C\rightarrow 2K+2K_2CO_3+3H_2 \qquad (1)$$

$$K_2CO_3\rightarrow K_2O+CO_2 \qquad (2)$$

$$CO_2+C\rightarrow 2CO \qquad (3)$$

$$K_2CO_3+2C\rightarrow 2K+3CO \qquad (4)$$

$$K_2O+C\rightarrow 2K+CO \qquad (5)$$
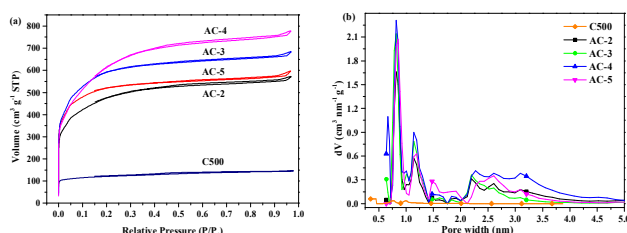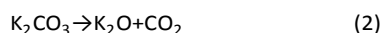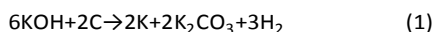
Fig. 3. (a) N_2 adsorption-desorption isotherms; (b) Pore size distributions of the nitrogen-enriched AC samples activated at different activating agent/precursor ratio.

Table 1. Textural properties of nitrogen-enriched AC samples

Sample	S_{BET}[§] $(m^2\,g^{-1})$	V_{tot}[§§] $(cm^3\,g^{-1})$	V_{mi}[§§§] $(cm^3\,g^{-1})$	V_{me}[§§§§] $(cm^3\,g^{-1})$
AC-2	1498	0.914	0.727	0.611
AC-3	1758	1.169	0.893	0.631
AC-4	1826	1.242	0.964	0.737
AC-5	1672	0.962	0.785	0.799

To investigate the nitrogen content and the doping configuration of nitrogen in AC, elemental analysis and XPS analysis were employed. The bulk elemental compositions of all samples were obtained by CHN combustion method, which are summarized in Table 2. From Table 2, it can be seen that, with the KOH/carbonization ratio (from 2:1 to 5:1) increase, the carbon and nitrogen contents of the AC samples decrease accompanied by a textural development in the ACs obtained, which can be demonstrated by the results of specific surface shown in Table 1. The nitrogen contents evaluated from the elemental analysis are 2.86, 2.38, 1.93, and 1.32 wt.% in AC-2, AC-3, AC-4 and AC-5, respectively. This means it is difficult to obtain a high porosity and a high nitrogen content at the same time for the activated carbons, since there was a substantial detriment to the nitrogen-containing functional groups due to oxidation during the activation process.[45] Accordingly, the surface chemical properties of the as-prepared ACs were analyzed by X-ray photoelectron spectroscopy (XPS), and the resulting spectra are shown in Fig. 4. XPS analysis reveals the bonding of N with C and the existence of four types of N (N-5,

N-6, N-Q, and N-X). Nitrogen atoms can be assigned to four different environments in the carbons: pyridinic-type nitrogen (N-6, 398.1 eV), which is sp^2 bonded to two carbon atoms and donates one p electron to the aromatic system; pyrrolic-type nitrogen (N-5, 399.5 eV) associated with phenolic or carbonyl groups on the neighboring carbon atoms of the five-member ring; quaternary-type nitrogen (N-Q, 400.7 eV), which is bonded to three carbon atoms in the central or valley position of the graphite layer; and oxidized nitrogen (N-X, 402 eV).[46, 47] The relative contents of these different functionalities in N 1s are shown in Fig. 4 and summarized in Table 2. Apparently, although the nitrogen content decreases with increasing the KOH/carbonization weight ratio, the N-6 and N-5 are predominant in all nitrogen-enriched activated carbons. This is because the carbon atoms on edges or defect sites in the plane are much more chemically active than those within the perfect plane and hence can be easily substituted by nitrogen atoms. According to the literature,[48] N-6 and N-5 with nitrogen located at the edges of graphite layers are considered to the responsible for the pseudo-capacitance effect, while the N-Q with positive charges can actively affect electron transfer through the carbon frameworks. Meanwhile, from Table 2, it can be seen that there is a decrease in N-6 and N-5 and an increase in N-Q and N-X as the increase of activating agent/precursor ratio. It may be caused by burning off the carbon networks with the increasing of KOH, resulting in the carbon atoms inside were break by KOH.

Table 2. Elemental analysis and the deconvolution of N 1s.

Sample	C (wt.%)	H (wt.%)	N (wt.%)	N 1s (at.%)			
				N-6	N-5	N-Q	N-X
AC-2	89.28	0.61	2.86	17.07	54.83	25.13	2.96
AC-3	86.24	0.96	2.38	8.32	51.06	28.44	12.18
AC-4	85.66	1.77	1.93	7.93	50.01	28.88	13.18
AC-5	82.06	2.29	1.32	7.18	48.94	29.86	14.02
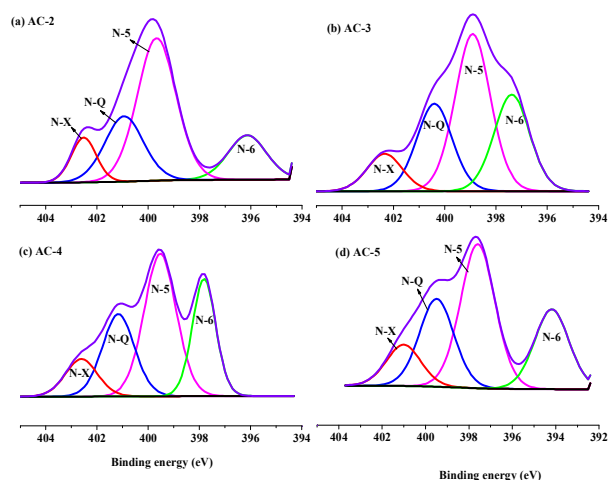
Fig. 4. N 1s line scan of nitrogen-enriched AC samples.

COMMUNICATION

Electrochemical characterization

In order to evaluate the electrochemical characteristics of the obtained ACs, CV, galvanostatic charge/discharge and EIS measurements were employed to characterize the capacitive properties in 7 mol L^{-1} KOH aqueous electrolytes in a symmetrical two-electrode cell. As shown in Fig. 5 and Fig. 6, the AC prepared at different activating agent/precursor ratio shows different capacitive behavior in CV and galvanostatic charge-discharge curves. The CV profiles obtained for AC-3, AC-4, and AC-5 are symmetric and rectangular in shape, typically being shown by EDLC with negligible internal cell resistance. AC-2 shows relatively high internal cell resistance, as evidenced by shifting from vertical change in current density on altering the electrode polarity near at 0 V and 1 V. It may be caused by increase in electrical resistivity in AC-2 due to the short of structural connectivity caused by insufficient activation. This is evident from substantial decrease in the volume of micropores in pore distribution analysis. Besides, it should be mentioned that as the scan rate increases, the CV curves gradually become depressed whilst maintaining a quasi-rectangular shape with slight distortions at high scan rates, which is mainly due to the resistance of the electrode. In Fig. 5(b), it can be seen that the rectangular CV shape of AC-3 is also maintained superbly at higher potential scan rates of 100 mV s^{-1} and 200 mV s^{-1}. The sample AC-2 shows a rectangular-like CV curve with a prominent redox peak in a wide voltage range of 0-0.7 V, while its V-t curve has an obvious deviation from linear shape at lower potential. This phenomena imply the presence of outstanding pseudo-capacitance effects. As nitrogen functional groups are electrochemically active to provide pseudo-capacitance, it can be assumed that the large pseudo-capacitance has mainly arisen from the large content of nitrogen functionalities attached to the carbon network. X.S. Du et al.[49] used nitrogen-doped graphene sheets to improve the electrochemical performance of graphene materials and found that the improved electrochemical performance of nitrogen-doped graphene sheets can be attributed to the functionalization effect of N-doping, which donates electron density to the aromatic rings of the graphene sheets and increases their conductivity. As the activating agent/precursor ratio increases, the deviations in CV and V-t curves become weakened, indicating that the relative contribution of pseudo-capacitance becomes smaller, which can be explained by the increased BET surface area (Table 1)
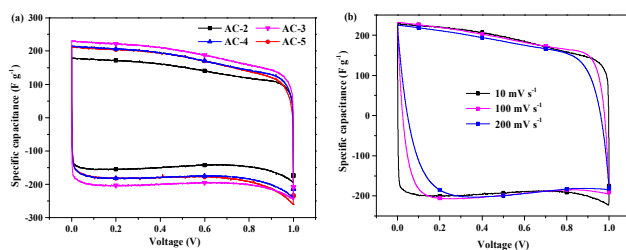
and decreased nitrogen content (Table 2).

Fig. 5. Cyclic voltammtry curves of nitrogen-enriched AC-based electrodes. (a) at a scan rate of 5 mV s^{-1} for all samples; (b) at different scan rates for AC-3.

Fig. 6(a) shows the galvanostatic charge/discharge curves of AC samples at the current densities of 0.05 A g^{-1} and the galvanostatic charge/discharge curves of AC-3 at various current densities from 0.05 to 1 A g^{-1}. All AC samples exhibits quasi-triangular galvanostatic charge/discharge curves with good symmetry, even at a high current density of 1 A g^{-1}, indicating excellent capacitive performance and electrochemical reversibility. A little deviation from the line in the work voltage-time curves correlates with the well-broadened redox 'hump' in the CV curves, further indicating the presence of pseudo-capacitance.

Fig. 6(b) shows a plot of specific capacitance versus current density for AC-2, AC-3, AC-4, and AC-5, whose specific capacitance are 198, 263, 255, and 241 F g^{-1} at a current density of 0.05 A g^{-1}, respectively. AC-3 has a highest specific capacitance though AC-4 has the highest surface area and the most pore volume, this is because high specific capacitance of AC-3 can be attributed not only to the relatively high surface area, but also to a large number of nitrogen functional groups. Nitrogen has higher electronegativity than carbon and can provide a lone electron pair for conjugation with the π-conjugated rings, which make the surface of the carbon materials more electrochemically active.[50-55] Previous studies have proposed that the pseudo-capacitance of the nitrogen-doped carbon in acidic medium probably comes from the following electrochemical reactions on the carbon surface:[6, 56]

$$-CNH + 2e^- + 2H^+ \leftrightarrow -CH-NH_2 \qquad (6)$$
$$-C-NHOH + 2e^- + 2H^+ \leftrightarrow -C-NH_2 + H_2O \qquad (7)$$
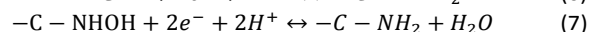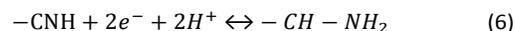
The redox reactions based on the protonation of nitrogen atoms at the edges and defect sites of graphitic domains (N-6 and N-5) could enhance the capacitance greatly with the pseudo-capacitance. However, Andreas and Conway [57] concluded that even though pseudo-capacitance in basic electrolyte is evident, its mechanism remains unclear. In base, the higher capacitance of AC samples were most likely the consequence of pseudo-capacitance due to the nitrogen atoms of pyridine groups and pyrrole groups, which represent more than 50% of all nitrogen atoms present on the surface. The electronic structure of these groups and the conjugation of the p-electrons seem to be the keys for obtaining high-performance electrode material for supercapacitors in basic electrolyte. Besides, it should be mentioned that as the current density increases, the IR drop can be readily seen increases, but this increase is more prominent in AC-2, AC-4, and AC-5 than AC-3. Lower increase in IR drop at higher current density means lower dissipation of capacitance in terms of heat. For example, as the current density increases from 0.05 to 5 A g^{-1}, the capacitance of AC-5 retains only 79.7% while AC-3 can retain as high as 86.7%, i.e. the capacitance loss in only 13.3%. The improved rate capability of the carbon may be related to the lower contribution of pseudo-capacitance, which has weaker endurance at large current density than double layer capacitance because of electrochemical polarization.

COMMUNICATION
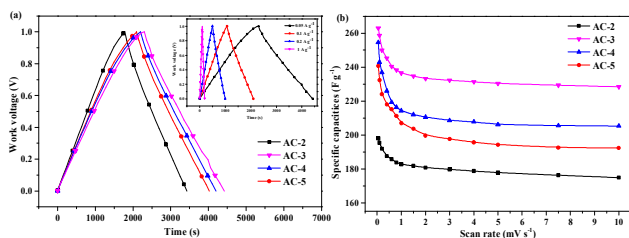
Fig. 6. (a) Galvanostatic charge-discharge curves of all samples at a current density of 0.05 A g^{-1} (insert: galvanostatic charge-discharge curves of AC-3 at different current densities; (b) The specific capacitance change of all AC electrodes as a function of current density.

EIS measurements were performed to clarify the kinetics within the electrode, as well as to evaluate the contribution of the heteroatom functionalities to the EDCL. The Nyquist plots for all AC samples in Fig. 7 comprise two parts: the straight line in low-frequency region and the semicircle in high-frequency region. It is well accepted that the semicircle in the impedance spectrum reflects the electrochemical reaction impedance, and smaller diameter of the semicircle means smaller charge transfer resistance.[58] As expressed by the diameters of the semicircles appear in the high frequency, the AC-2 (about 0.4) electrodes have large charge transfer resistance than that of AC-3, AC-4, and AC-5 (about 0.17, 0.16, and 0.15, respectively), indicative of more redox reactions that agrees well with the CV curves. The near-vertical line in the low-frequency region of Nyquist plot for the AC-2 electrode indicates fast ion diffusion due to its enhanced wettability of surface that resulted from the nitrogen functional groups.
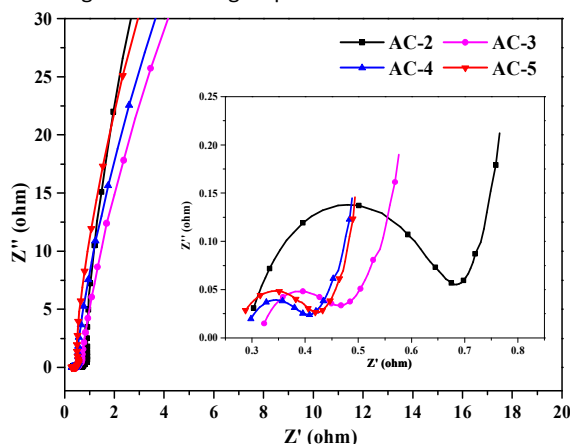
Fig. 7. Nyquist plots (insert: enlarge high-frequency region of Nyquist plots).

High durability is a highly required parameter for electrode materials to endure good structural integrity over long term operation. To check this performance, all of the nitrogen-enriched AC electrodes were tested for 3000 cycles of galvanostatic charge/discharge at a constant current density of 5 A g^{-1}. Fig. 8 shows that all of the AC samples have retained over 95% of initial capacitance up to 3000 charge/discharge cycles, indicating the good cycle durability of nitrogen-

enriched AC samples and confirming that the pseudo-capacitance introduced by nitrogen-containing functionalities is very stable with cycling.
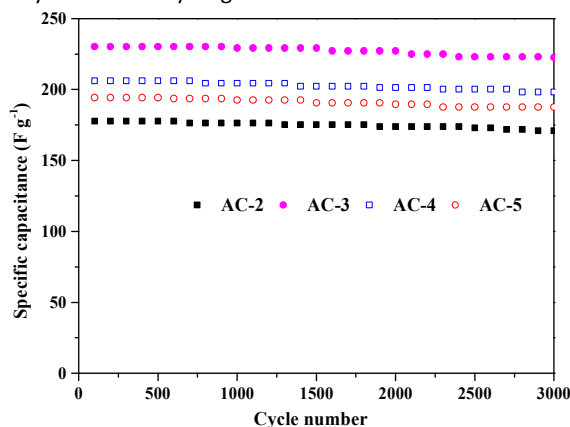
Fig. 8. Capacitance retention as a function of cycle number for all samples at a current density of 5 A g^{-1}.

Conclusions

We have presented a simple and scalable method to fabricate enriched-nitrogen activated carbons (2.9 ~ 1.3 *wt*.%) by direct heat treatments of waste particleboards for high-performance supercapacitors which manifestes an easy and efficient conversion of an agricultural and forestry waste material to a value-added material. The surface concentration of heteroatom, chemical structure, and surface area highly depend on the activating agent/precursor ratio. As the weight ratio of KOH/carbonization increases from 2 to 5, the specific surface area increases from 1498 to 1826 m^2 g^{-1}, while the nitrogen content decreases from 2.86 to 1.32 *wt*.%. The obtained activated carbons were tested as supercapacitor electrodes in 7 mol L^{-1} KOH aqueous electrolytes in a symmetrical two-electrode cell. All the activated carbons showed excellent performance in terms of specific capacitance and durability at high current density and for long term operation. The activated carbon prepared at 3:1 ratio of KOH and the pre-carbonized char has shown the best performance with specific capacitance of 263 F g^{-1} at 0.05 A g^{-1} and retained up to 228 F g^{-1} at 10 A g^{-1} current density. The high contents of nitrogen functional groups are found to be critical to obtain the optimal electrochemical performance. The nitrogen-enriched activated carbon electrodes prepared with a moderate KOH/carbonization weight ratio of 3 exhibits high gravimetric specific capacitances, good rate capability, excellent lone-term stability, and extended potential window, making such electrode material a promising candidate for supercapacitors. Therefore, it can be optimize the electrochemical performance of supercapacitors through the regulation and control of the activating agent/precursor ratio.

Acknowledgements

COMMUNICATION

Notes and references

§S_{BET}: BET surface area.
§§ V_{tot}: total pore volume (less than 465 nm pore size).
§§§ V_{mi}: micropore volume (below 2 nm pore size).
§§§§ V_{me}: mesopore volume (between 2 nm and 50 nm pore size).

1   B.E. Conway, Kluwer Academic/Plenum, New York, 1999.
2   M. Winter and R.J. Brodd, Chem. Rev., 2004, 104, 4245-4269.
3   S. Patrice and Y. Gogotsi, Nat. Mater., 2008, 7, 845-854.
4   Y.P. Zhai, Y.Q. Dou, D.Y. Zhao, P. F. Fulvio, R.T. Mayes and S. Dai, Adv. Mater., 2011, 23, 4828 -4850.
5   W.J. Qian, F.X. Sun, Y.H. Xu, L.H. Qiu, C.H. Liu, S.D. Wang and F. Yan, Energy Environ. Sci., 2014, 7, 379 -386.
6   M. Zhou, F. Pu, Z. Wang and S.Y. Guan, Carbon, 2014, 68, 185-194.
7   Y.R. Liang, F.X. Liang, H. Zhong, Z.H. Li, R.W. Fu and D.C. Wu, J. Mater. Chem. A, 2013, 1, 7000-7005.
8   H. Zhu, X.L. Wang, X.X. Liu and X.R. Yang, Adv. Mater., 2012, 24, 6524-6529.
9   G.P. Wang, L. Zhang and J.J. Zhang, Chem. Soc. Rev., 2012, 41, 797-828.
10 G.A. Snook, P. Kao and A.S. Best, J. Power Sources, 2011, 196, 1-12.
11 Z.S. Wu, D.W. Wang, W.C. Ren, J.P. Zhao, G.M. Zhou, F. Li and H.M. Cheng, Adv. Funct. Mater., 2010, 20, 3595-3602.
12 S. Chen, J.W. Zhu, X.D. Wu, Q.F. Han and X. Wang, ACS Nano, 2010, 4, 2822-2830.
13 A. Sumboja, C.Y. Foo, X. Wang, and P.S. Lee, Adv. Mater., 2013, 25, 2809-2815.
14 M. Anouti and L. Timperman, Phys. Chem. Chem. Phys., 2013, 15, 6539-6548.
15 M.J. Zhi, C.C. Xiang, J.T. Li, M. Li and N.Q. Wu, Nanoscale, 2013, 5, 72-88.
16 Y.Y. Lv, F. Zhang, Y.Q. Dou, Y.P. Zhai, J.X. Wang, H.J. Liu, Y.Y. Xia, B. Tu and D.Y. Zhao, J. Mater. Chem., 2012, 22, 93-99.
17 B. Xu, S.F. Yue, Z.Y. Sui, X.T. Zhang, S.S. Hou, G.P. Cao and Y.S. Yang, Energy Environ. Sci., 2011, 4, 2826-2830.
18 D. Hulicova-Jurcakova, A.M. Puziy, O.I. Poddubnaya, F. Suárez-García, J.M.D. Tascón and G.Q. Lu, J. Am. Chem. Soc., 2009, 131, 5026-5027.
19 B. Xu, H. Duan, M. Chu, G.P. Cao and Y.S. Yang, J. Mater. Chem. A, 2013, 1, 4565-4570.
20 C.Z. Yuan, B. Gao, L.F. Shen, S.D. Yang, L. Hao, X.J. Lu, F. Zhang, L.J. Zhang and X.G. Zhang, Nanoscale, 2011, 3, 529-545.
21 E. Raymundo-Piñero, M. Cadek and F. Béguin, Adv. Funct. Mater., 2009, 19, 1032-1039.
22 X.L. Wu, W. Wang, Y.G. Guo and L.J. Wan, J. Nanosci. Nanotechnol., 2011, 11, 1897-1904.
23 N. Gavrilov, I.A. Pašti, M. Vujković, J. Travas-Sejdic, G. Ćirić-Marjanović, and S.V. Mentus, Carbon, 2012, 50, 3915-3927.
24 N. Gavrilov, M. Vujković, I.A. Pašti, G. Ćirić-Marjanović and S.V. Mentus, Electrochim. Acta, 2011, 56, 9197-9202.
25 A. Janošević, I. Pašti, N. Gavrilov, S. Mentus, J. Krstić, M. Mitrić, J. Travas-Sejdic and G. Ćirić-Marjanović, Microporous Mesoporous Mater., 2012, 152, 50-57.
26 A. Janošević, I. Pašti, N. Gavrilov, S. Mentus, G. Ćirić-Marjanović, J. Krstić and J. Stejskal, Synth. Met., 2011, 161, 2179-2184.
27 D.S. Yuan, T.X. Zhou, S.L. Zhou, W.J. Zou, S.S. Mo and N.N. Xia, Electrochem. Commun., 2011, 13, 242-246.
28 M.M. Yang, B. Cheng, H.H. Song and X.H. Chen, Electrochim. Acta, 2010, 55, 7021-7027.
29 J.B. Yin, X. Xia, L.Q. Xiang and X.P. Zhao, Carbon, 2010, 48, 2958-2967.
30 W. Kim, M.Y. Kang, J.B. Joo, N.D. Kim, I.K. Son, P. Kim, J.R. Yoon and J. Yi, J. Power Sources, 2010, 195, 2125-2129.
31 X.Y. Chen, C. Chen, Z.J. Zhang, D.H. Xie, X. Deng and J.W. Liu, J. Power Sources, 2013, 230, 50-58.
32 K. Jurewicz, R. Pietrzak, P. Nowicki and H. Wachowska, Electrochim. Acta, 2008, 53, 5469-5475.
33 P. Girods, A. Dufour, V. Fierro, Y. Rogaume, C. Rogaume, A. Zoulalian and A. Celzard, J. Hazard. Mater., 2009, 166, 491-501.
34 Y.L. Lv, China Forestry Industry, 2014, 4, 36-38.
35 Z.H. Huang and Y.L. Wang, China Forest Products Industry, 2005, 32, 16-19.
36 P. Girods, Y. Rogaume, A. Dufour, C. Rogaume and A. Zoulalian, Renew. Energ., 2008, 33, 648-654.
37 T. Nakai, S. N. Kartal, T. Hata and Y. Imamura, Build. Environ., 2007, 42, 1236-1241.
38 A.C. Ferrari, J.C. Meyer, V. Scardaci, C. Casiraghi, F. Mauri, S. Piscanec, D. Jiang, K.S. Novoselov, S. Roth and A.K. Geim, Phys. Rev. Lett., 2006, 97, 187401.
39 M. Zhou, T.W. Cai, F. Pu, H. Chen, Z. Wang, H.Y. Zhang and S.Y. Guan, ACS Appl. Mater. Interfaces, 2013, 5, 3449-3455.
40 M.L. Liu, L.H. Gan, W. Xiong, F.Q. Zhao, X.Z. Fan, D.Z. Zhu, Z.J. Xu, Z.X. Hao and L.W. Chen, Energy Fuels, 2013, 27, 1168-1173.
41 W. Xing, C.C. Huang, S.P. Zhuo, X. Yuan, G.Q. Wang, D. Hulicova-Jurcakova, Z.F. Yan and G.Q. Lu, Carbon, 2009, 47, 1715-1722.
42 B.B. Garcia, S.L. Candelaria and G.Z. Cao, J. Mater. Sci., 2012, 47, 5996-6004.
43 G.Q. Lu, X.S. Zhao and T.K. Wei, London, 2004.
44 J.C. Wang, and S. Kaskel, J. Mater. Chem., 2012, 22, 23710-23725.
45 L. Zhao, L.Z. Fan, M.Q. Zhou, H. Guan, S.Y. Qiao, M. Antonietti, and M. Titiric, Adv. Mater., 2010, 22, 5202–5206.
46 F.B. Su, C.K. Poh, J.S. Chen, G.W. Xu, D. Wang, Q. Li, J.Y. Lin and X.W. Lou, Energy Environ. Sci., 2011, 4, 717-724.
47 T.X. Shang, X.X. Cai and X.J. Jin, RSC Adv., 2015, 5, 16433-16438.
48 D. Hulicova-Jurcakova, M. Seredych, G.Q. Lu and T.J. Bandosz, Adv. Funct. Mater., 2009, 19, 438-447.
49 X.S. Du, C.F. Zhou, H.Y. Liu, Y.W. Mai and G.X. Wang, J. Power Sources, 2013, 241, 460-466.
50 Z. Li, Z.W. Xu, X.H. Tan, H.L. Wang, C.M.B. Holt, T. Stephenson, B.C. Olsen and D. Mitlin, Energy Environ. Sci., 2013, 6, 871-878.
51 Z.S. Wu, W.C. Ren, L. Xu, F. Li and H.M. Cheng, ACS Nano, 2011, 5, 5463-5471.
52 D. Bhattacharjya, H.Y. Park, M.S. Kim, H.S. Choi, S.N. Inamdar and J.S. Yu, Langmuir, 2014, 30, 318-324.
53 L. Chen, Y.Z. Zhang, C.H. Lin, W. Yang, Y. Meng, Y. Guo, M.L. Li and D. Xiao, J. Mater. Chem. A, 2014, 2, 9684-9690.
54 T. Nakajima, M. Koh and M. Takashima, Electrochim. Acta, 1998, 43, 883-891.
55 Y.P. Wu, S.B. Fang and Y.Y. Jiang, Solid State Ionics, 1999, 120, 117-123.
56 D. Hulicova-Jurcakova, M. Kodama, S. Shiraishi, H. Hatori, Z.H. Zhu and G.Q. Lu, Adv. Funct. Mater., 2009, 19, 1800-1809.
57 H.A. Andreas and B.E. Conway, Electrochimica. Acta, 2006, 51, 6510-6520.
58 L. Yang, S. Cheng, Y. Ding, X.B. Zhu, Z.L. Wang and M.L. Liu, Nano Lett., 2012, 12, 321-325.